Interaction of ocean wave energy converters

van Vlijmen, Bruis; Goudswaard, Reinier; Boere, Remco ; Schneider, Thomas; Polinder, Henk; Lavidas, George

Publication date
2019

Document Version
Final published version

Published in
Proceedings of the 13th European Wave Energy and Tidal Conference (EWTEC 2019)

13th ewtec 2019 Proceedings of the 13th European Wave and Tidal Energy Conference 1-6 Sept 2019, Naples, Italy

Interaction of Ocean Wave Energy Converters

Bruis van Vlijmen, Reinier Goudswaard, Remco Boere, Thomas Schneider,
Henk Polinder and George Lavidas

***Abstract*—It is expected that several identical Point Absorber Wave Energy Converters (PAWECs) will be arranged in arrays to form a Wave Energy Farm. One of the key challenges in designing such a WEC array is their spatial configuration, as the WECs in the farm interact hydrodynamically with each other. This study focuses on different potential PAWEC deployments to identify the best relative position in order to maximise energy output. This is done by resolving the hydrodynamic interactions between a modelled WEC point absorber, with use of open-source Boundary Element Methods (BEM) and time domain WEC simulator. The results from the numerical model are also compared with wave tank testing, to verify the accuracy of the analysis. The simulations show that the relative position can significantly increase a WEC's individual power output. A spatial pattern of relative positions that result in higher potential power extraction was shown, with increases up to 20% compared to a single WEC on its own. However, the computational results showed realistic results for only a select number of configurations. As for the experiment, unexpected variations in test conditions occurred, inhibiting the possibility to isolate certain events. Therefore, when cross checking results from both simulations and experiments, the identified simulated trends only partially showed adherence with the experimental data. Henceforth, the knowledge gathered from the simulations can't conclusively be validated by the experiments conducted in this study. This study shows that the spatial configuration of two WECs influences their individual power outputs.**

***Index Terms*—Wave Energy, Point Absorber, Hydrodynamic Interaction, boundary element method solvers, NEMOH, WEC-Sim.**

NOMENCLATURE

α	Angle of relative WEC location to x-axis
$\bar{P}$	Power output of a WEC normalized with respect to (wave height)^2
η	Free surface deflection
$\vec{V}$	Velocity
Φ	Velocity Potential
ρ	Density of seawater
B_{PTO}	Damping Constant of Power Take Off system
g	Constant of gravity
H	Wave Height - trough to peak
P	Power output of a WEC
p	Pressure
q	q-factor, individual power output of an interacting WEC divided by power output of an isolated WEC
r	Relative Distance between WECs
R^2	Coefficient of determination for WEC
T	Wave Period

Paper ID: 1568
Conference track: WDD

B. van Vlijmen was at Delft University of Technology, Mechanical Engineering Department. He is now with Stanford University, (MSc.) Mechanical Engineering Department.(email: bvlijmen@stanford.edu

R. Goudswaard was at Delft University of Technology, Mechanical Engineering Department. He is now with Delft University of Technology, (MSc.) Aerospace Engineering Department. (email: reinier-goudswaard@hotmail.com)

R. Boere was at Delft University of Technology, (BSc.) Mechanical Engineering Department. He is now with Delft University of Technology, (MSc.) Mechanical Engineering Department.(email: r.boere@hotmail.com)

T. Schneider was at Delft University of Technology, Mechanical Engineering Department. He is now with Imperial College, (MSc.) Mechanical Engineering Department.(email: thomas-paul.schneider@orange.fr)

H. Polinder is an Associate Professor and head of the Ocean Energy Group at the TU Delft (e-mail: H.Polinder@tudelft.nl)

G. Lavidas was a researcher at the University of Edinburgh and is now a Marie Skoldowska Curie Fellow at TU Delft (e-mail: g.lavidas@tudelft.nl)

I. INTRODUCTION

ONE of the largest challenges that humanity will face in the current century is the transition from fossil fuels to renewable energy resources.Harnessing the wave energy from the world's oceans could potentially be one of the solutions. It is estimated that the total global wave power resource is 2.11 TW, which would offer significant benefits in the decarbonisation of our societies [1], [2]. However, WEC's are not yet utilising the untapped wave potential due in part in high capital expenditure and uncertainties in energy production.

Over the last decade, the number of wave energy research and commercialization projects has grown increasingly. Most of these projects seem to converge to a one type of technology to extract ocean energy: arrays of axi-symmetric Point Absorber WECs (PAWEC), consisting of dozens of WEC units [3], with a typical power output of 0.25 - 1 MW per device [4].

Having multiple of such oscillating bodies in close spatial configuration, could bring about hydrodynamic interactions due to oscillation-induced radiation and reflection waves. Shedding light on the significance of these interactions and learning how they can be influenced is important for energy corporations designing the spatial configuration of an offshore WEC array. Other works of academic literature have explored the influence of different spatial configurations on the power output of WEC arrays, both computationally and experimentally [5], [6]. Those studies focused on the effect in total energy output of as a result of different spatial configurations of the whole WEC array [7]. However, in order to gain more insight in the governing parameters and a robust understanding of this hydrodynamic interaction, this paper isolates that event and analyzes the behaviour of just two WEC units in close proximity.

This paper aims to identify how the spatial configuration of two generic WECs impact their individual power output.

The study analyses the reciprocal dynamic behaviour utilizing linear potential flow theory, specifically the Boundary Element Method (BEM). Utilising the BEM in the frequency domain the effects of wave radiation and diffraction around the WEC are captured. Subsequently, the power output of the two WEC units is computed using a WEC Simulation software tool, in time domain. Based on these analyses, the relative locations where the WEC units experience higher and lower levels of individual power output are indicated for various wave conditions.

Finally, building upon the modeling analysis a physical experiment, with two WEC point absorbers, is performed at the wave tank of TU Delft, in order to validate the behaviour of the findings.

II. Materials and Methods

A. System description

(A.1) WEC device: As heave Point Absorber WEC units are growing to become the most widely used technology for wave energy extraction in arrays, these are the type of WEC that we consider for further analysis. This WEC design will be referred to as 'a typical WEC'. Based on literature review the typical WEC is taken to be an axi-symmetric semi-submerged cylinder with a draft of 2m and a diameter of 10m [4], [6], [8].

The power take off (PTO) system is designed to be a viscous damper with a fixed damping constant $B_{PTO} = 810$ kNm/s, enabling the WEC to operate at 90% of its peak power output at all of the investigated wave conditions. These values were determined by running several preliminary simulations for the four different wave conditions. A schematic depiction of such a WEC is shown in Figure 1.

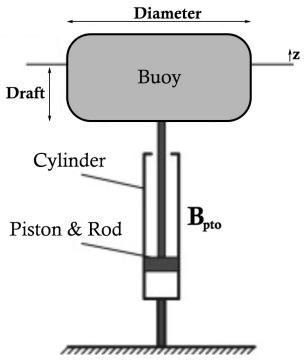

Fig. 1. Schematic image of a typical (Point Absorber) WEC according to literature [4], [6], [8].

(A.2) Wave conditions: Investigation is limited to Point Absorbers that extract energy in heave direction. Therefore, deep sea conditions, implying vertical circulatory motion of the water, are maintained throughout all analyses. To simplify the computational and experimental method and to isolate the dynamic behaviour in heave direction, the movement of WEC is limited to 1 degree of freedom (DOF) in vertical direction.

TABLE I
Chosen experimental wave conditions

Wave Condition	Wave Height [m]	Period [s]
Weak	2.5	7.0
Fair	3.5	8.0
Moderate	3.5	9.0
Rough	4.5	10.0

Lower bounds are defined by energy density. Higher bounds are defined by physical limitations of wave tank.

The power output of the WECs is examined for 4 different wave conditions, see Table I. The conditions are based on the joint prabibility distribution by the ossurence matrix, by measurements from a site located at the Atlantic coast [9].

(A.3) Array configuration: To provide insight into the behaviour of a complete array of dozens of WECs, the dynamic problem is isolated to only two WECs. Various spatial configurations are characterised by the relative location of one WEC to the other. Using a polar coordinate system, the relative location of the two WECs is described by distance r and angle α, see Figure 2, with incoming waves parallel to the x-axis.

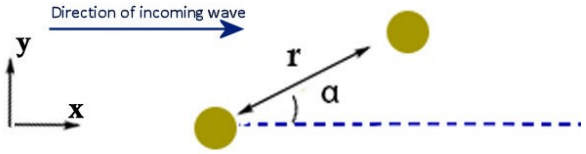

Fig. 2. A top view schematic of the relative position. The circle on the left represents WEC 1, the other circle is WEC 2.

B. Computational method

The fundamental equations and theories that are used in our computational models are gathered from a collection of hydromechanics literature sources [10], [11] and Boundary Element Method specific literature [12].

(B.1) Linear Potential Flow Theory: To characterize the hydrodynamic response of a WEC in monochromatic waves, linear potential flow theory is assumed to describe the fluid-structure interaction on a floating body.

The theory describes the fluid velocity, $\overrightarrow{V}$ as the gradient of the potential flow $\Phi(x, y, z, t)$.

$$\overrightarrow{V} = \bigtriangledown\Phi \tag{1}$$

Following the potential flow theory, assumptions are made that the fluid surrounding the body is a homogeneous, incompressible and inviscid fluid. Furthermore, surface tension may be neglected.

Using the assumption of homogeneity and incompressibility the equation of conservation of mass reduces to the equation of continuity:

$$\frac{\delta \rho}{\delta t} = - \bigtriangledown \cdot (\rho \overrightarrow{V}) \tag{2}$$

$$\frac{\delta V_x}{\delta x} + \frac{\delta V_y}{\delta y} + \frac{\delta V_z}{\delta z} = 0 \tag{3}$$

Here V_x,V_y and V_z are the velocity components of Cartesian directions x, y and z in space and time.

As inviscid fluid conditions are assumed, this implies irrotationality, as there is no (or constant) vorticity. Due to irrotationality the following can be said about the velocity potential which satisfies the Laplace equation.

$$\bigtriangledown \times \overrightarrow{V} = 0 \ \ and \ \ \bigtriangledown^2 \Phi = 0 \tag{4}$$

Substituting the relationship between potential and velocity into equation 3 we arrive at the rewritten form of the Laplace equation:

$$\frac{\delta^2 \Phi}{\delta x^2} + \frac{\delta^2 \Phi}{\delta y^2} + \frac{\delta^2 \Phi}{\delta z^2} = 0 \tag{5}$$

The velocity potential can be substituted in the Bernoulli equation, which yields the unsteady Bernoulli equation.

$$\rho \frac{\delta \Phi}{\delta t} + \frac{1}{2}(V\Phi^2) + p + \rho g z = c(t) \tag{6}$$

To reach a solution for Φ, consequently solving the unsteady Bernoulli equation, the boundary conditions are to be set. The seabed and body boundary conditions are linear, the free surface boundary condition is non-linear. The boundary conditions are defined as such:

Body Boundary Conditions: The velocity of the water and the velocity of the body, on the wet surface are equal.

$$\overrightarrow{V}_{wet} = \overrightarrow{V}_{flow} \tag{7}$$

Next are the **Sea Bed Boundary Conditions**, were naturally there is impermeability and no fluid perturbation. As infinite depth is assumed, the following boundary condition is set:

$$\frac{\delta \Phi}{\delta z} = 0 \ \ at \ \ z = -\infty \tag{8}$$

The **Free Surface Boundary Condition** (FSC) is a non-linear boundary condition where the free surface position is not known beforehand. Two equations arise from the FSC, here $\eta(x,t)$ is the free surface deflection:

$$\frac{\delta \eta}{\delta t} + \bigtriangledown \eta \cdot \bigtriangledown \Phi = 0 \tag{9}$$

$$\frac{\delta \Phi}{\delta t} + g\eta + \frac{1}{2}(\bigtriangledown \Phi)^2 = 0 \tag{10}$$

The BEM solver used in this paper finds a first order linear approximation for the FSC [12] and solves the boundary value problems in frequency domain. This can be done only if small body motions around the mean positions are considered.

(B.2) Equations of motion: The equations of motion are used following the methodology used in Green's function [12].

$$m\ddot{X} = F_{exc}(t) + F_{rad}(t) + F_{PTO}(t) + F_{hydro}(t) \tag{11}$$

$F_{exc}(t)$, the excitation force, $F_{rad}(t)$, the radiation force, and $F_{hydro}(t)$, the resulting hydrodynamic force, are calculated using hydrodynamic coefficients which are provided by the frequency-domain BEM-solver. $F_{PTO}(t)$ is the force exerted by the Power Take Off system on the floating body.

(B.3) Numerical model: The choice for a numerical model was based on merits of availability (open-source) and suitability as a solver for boundary elements. The most suitable choice for a numerical model is to use the open source boundary element method (BEM) solver NEMOH [12]in combination with the time-domain solver WEC-Sim [13].

With these numerical models, two sets of simulations were conducted: a general simulation for investigating the influence on the spacial configuration of the WECs and a specific simulation, used for the comparison with the experiments.

C. Experimental method

The experiment was devised with the main objective to validate any trends identified from the computational results. The towing tank at TU Delft was utilized to simulate realistic wave conditions. The 85m long wave tank has a width of 2.75m and depth of 1.20m, it is pictured in Figure 3. It was decided to use a scaling factor of 1:40, based on the physical limitations of the facility such as the requirements to assume deep sea conditions.

Fig. 3. Towing tank No.2, a wave maker facility of the Maritime & Transport Technology of TU Delft.

(C.1) Test set up: The two 1:40 scale WEC models were made based on the dimensions of the design as described in II-A (see Figure 4). The required 1 DOF vertical movement of the WECs is secured by mounting the buoy to a rod hanging in linear sliding bearings. The damping of the PTO system is realized by a viscous damper, with a designed damping coefficient of 80.

An elevation sensor was attached to the buoy to accurately measure its vertical position and consequently velocity. A load cell was used to connect the piston of the damper to the WEC in order to measure the forces applied by the damper. The combined data the elevation sensor and the load cell gives insight in both the damper characteristics and the power output of the entire system. Two complete WEC assemblies were

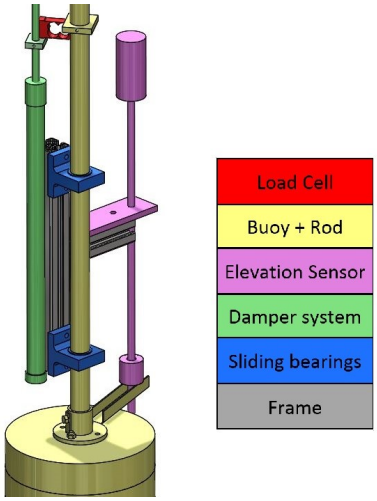

Fig. 4. Complete WEC assembly used in the experiment.

placed in the towing tank as illustrated in Figure 5. They were mounted in a frame of sliding aluminum beams, making it easy to adjust the two WECs' positions in the array. A small wave gauge was placed

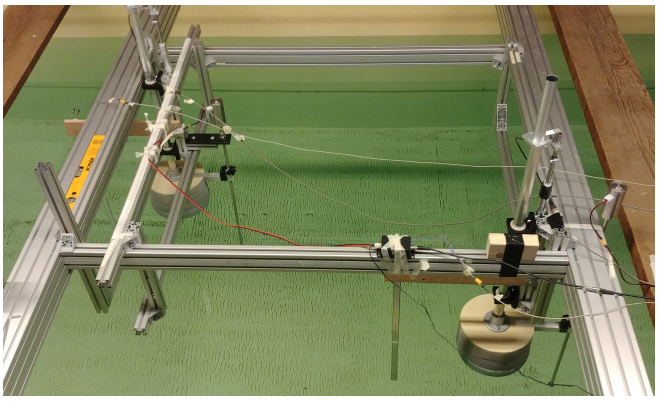

Fig. 5. Array of two complete WEC assemblies placed in the testing facility. The wave is incoming from the right.

0.25m behind every WEC measuring the water level, to provide insight in the wave height in the wake of the WEC. A bigger and more accurate wave gauge was placed 2.5m in front of the array to determine the characteristics of the incoming wave (see Figure 6).

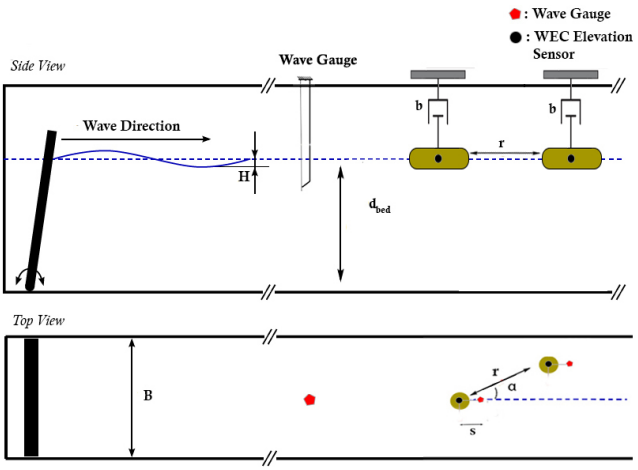

Fig. 6. Top View and Side View schematic representation of experimental setup.

(C.2) Test conditions: For the experiment 40 different test runs were conducted, each with a different test condition, consisting of a combination of 10 different array configurations and 4 different wave types. The array configurations were chosen based on trends identified during preliminary computational results of NEMOH and WEC-Sim.

The 10 different configurations consist of three sweeps as shown in Figure 7; *Sweep 1* with a constant angle of $\alpha = 30$ and four different radii, *Sweep 2* with a constant radius and four different angles, and *Sweep 3* with a constant angle of $\alpha = 90$ and three different radii.

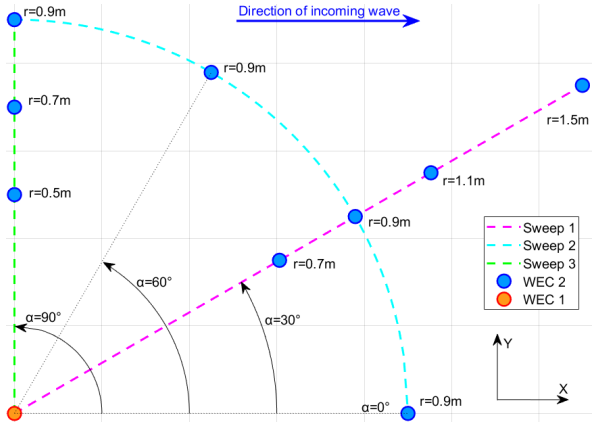

Fig. 7. Array configurations of the experiment.

As the wave tank's wall is relatively close to the array it was important to analyze its influence on the hydrodynamic behaviour of the WECs. Therefore, a separate set of wall-effect test runs was done in which the entire array was shifted to different distances from the wall for one specific array configuration ($\alpha = 90$, $r = 0.7$) and compared to the original results.

At last a set of test runs was done to determine the individual performance of each WEC, by placing only one WEC at the time in the middle of the wave tank.

It was decided to do tests runs for all of these array configurations for four different wave conditions as described in section II-A, scaled down with Froude.

III. Results

D. Computational results

For every wave condition (see II-A) a 2D color plot was made for both WEC 1 and WEC 2, showing the q-factor depending on the relative position of WEC 2. The q-factor is defined as the power output of a WEC in the array divided by the power output of an isolated WEC (P_{iso}) for the same wave conditions, as introduced by Barbarit (2010) [14]:

$$q = \frac{P}{P_{\text{iso}}} \tag{12}$$

Figures 8 and 9 show these results for fair wave conditions. The other wave conditions show similar trends. When the WECs are at $\alpha = 90$ their q-factors should be identical, being positioned next to each other. To visualize this without the averaging effects of the surrounding points an extra band was plotted at $X = 0$. This band is on the left side of each figure and as expected both are identical.

Figure 8 shows an increase of the power output of WEC 1 at circular bands, and a power decrease in the area's in between. This observation can likely be linked to the creation caused by the interference pattern of radiation waves created between both WECs. The effects are attenuated for greater distances.

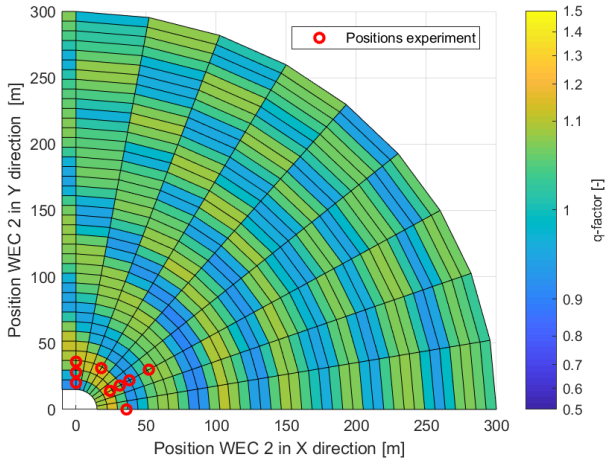

Fig. 8. q-factor of WEC 1 plotted against the relative position of WEC 2 for fair wave conditions.

Figure 9 shows vertical bands with counter-intuitive increase or decrease in power output of WEC 2, more than 50% less or more compared to a single WEC. As expected however, the power output for $X = 0$ is equal to that of WEC 1.

The above mentioned figures are summarized in Table II where the maximum power outputs are listed for each wave condition.

As mentioned, the color plots show remarkable behaviour for WEC 2. This is also illustrated in Figure 10, where a detailed comparison of the power output of the two WECs for angles $\alpha = 80$ and $\alpha = 90$ is shown. As mentioned above the q-factors at $\alpha = 90$ are identical. A large drop in power output is seen for WEC 2 at $\alpha = 80$ near a distance of 200.

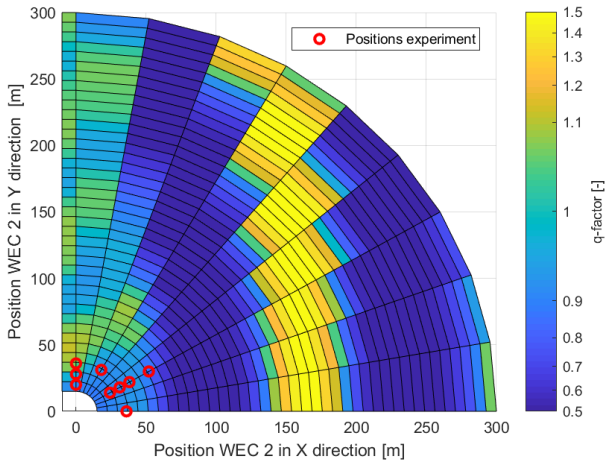

Fig. 9. q-factor of WEC 2 plotted against the relative position of WEC 2 for fair wave conditions.

TABLE II
SUMMARY OF COMPUTATIONAL RESULTS

Wave cond.	**WEC 1**		**WEC 2**	
	q [-]	P_{real} [kW]	q [-]	P_{real} [kW]
Weak	1.21	158	1.67	218
Fair	1.16	330	1.59	454
Moderate	1.09	311	1.89	538
Rough	1.08	483	1.57	708

Listing the changes in power outputs for WEC 1 and WEC 2. The maximum q-factor and real P are listed.

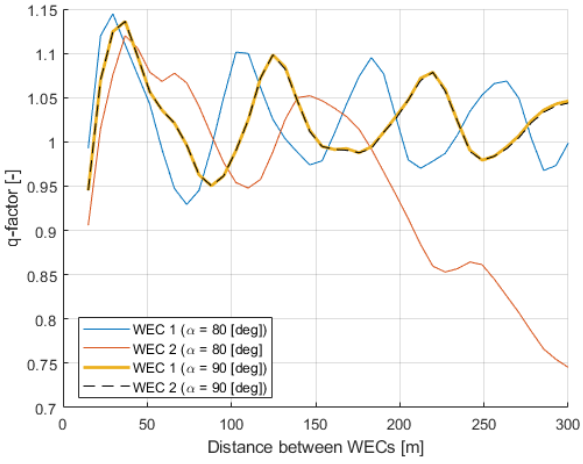

Fig. 10. q-factor for both WECs for angles $\alpha = 80$ and $\alpha = 90$.

.

E. Experimental results

(B.1) Deviation: For each test run, the waves produced by the wave maker was measured, and the average height was calculated. The mean and standard deviation of the average wave height are shown in Table III for the four wave conditions. The wave height is measured with a 1σ uncertainty of 0.2, but as there are a lot of measurement points, the error in the mean

TABLE III
ACTUAL EXPERIMENTAL WAVE CONDITIONS

Wave condition	Wave height [mm]	Standard deviation [mm]
Weak	60	4
Fair	89	5
Moderate	84	5
Rough	110	10

The measured mean and standard deviation of the produced wave heights for the four wave types. The standard deviation is the deviation between runs.

becomes negligible. Later, his assumption is also made for the load cells and elevation sensors.

Using the results of the set of individual performance experiments (see section II-C), the uncertainty between the measured and simulated power output for an individual WEC was found to be $\sigma_P = 0.05$. This was calculated by comparing a set of measured individual WEC power outputs with a set of simulations for the performance of individual point absorbers (not being in an array).

Lastly, the set of wall-effect experiments (see II-C) showed no clear correlation between the array to wall distance and the power performance, even though the results did show significant variance.

(B.2) Results: The results of the experiment are analyzed by comparing the experimental and computational power performances of both WECs for the three configuration *sweeps* (see II-C). The results of *Sweep 1* and *Sweep 2* for weak wave conditions are shown in Figure 11 and 12.

As can be seen in Table III, there is a large deviation in the mean wave height between runs, up to 9%. Therefore, it was decided to normalize the experimental power output by dividing it by the squared measured average wave height[1], and use a wave height of $1m^2$ in the simulations.

The first thing to notice is that the values of the computational results are always higher than those of the experiment. A possible explanation for this is that friction was not taken into account in the simulations, whilst a significant amount of power was lost due to friction of the sliding bearings. When looking at the trends of the curves of the simulation and experiment, they sometimes seem to agree, but for some they don't show much agreement. Noticeable is that in Figure 11 the measurements of WEC 1 and WEC 2 show the same trend, but the simulated curves of the two WECs are not alike at all.

For every experimental run, the damping constant of the damper system was calculated using the data of the load cell and the elevation sensor. For every simulated curve of Figure 11 and 12 the average damping constant of the four corresponding measurements was used. Taking this average would be an acceptable method if the damping constant has a small deviation, but Figure 13 shows the opposite. This means that the

[1]The numeric model showed quadratic relationship between power output and wave height.

[2]Valid because solver uses linear wave theory.

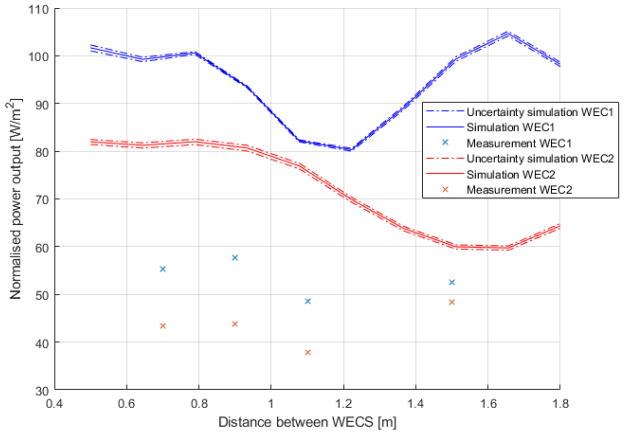

Fig. 11. Experimental and computational normalized power output of WEC 1 and WEC 2 for Sweep 1 ($\alpha = 30$) configurations with weak wave conditions.

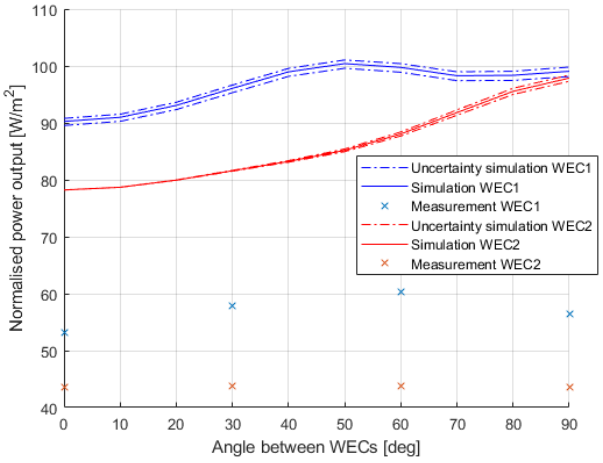

Fig. 12. Experimental and computational normalized power output of WEC 1 and WEC 2 for Sweep 2 configurations (r = 0.9) with weak wave conditions.

measurement points shown in Figure 11 and 12 have a very different damping constant whilst the graphs of the simulation have a constant damping.

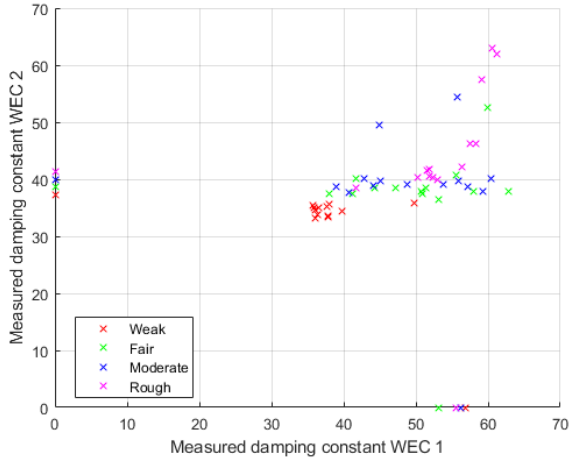

Fig. 13. Specific damping constant of WEC 1 and WEC 2 for every single run. Error bars became invisible due to large number of measurement points.

For a relevant comparison of the experimental and computational results it is crucial that all the parameters are identical. Therefore, it was decided to determine the wave height and damping constant per WEC for every single run, and use them to execute 48 simulations with identical conditions for each of the 48 runs. Figure 14 and 15 show a comparison of the measured and simulated power output for both WEC 1 and WEC 2, both at 1:40 scale. A perfect match of the experimental and computational results would result in a fitted curve through the origin with slope 1. The curve fits shown in Figure 14 and 15 however have an offset to the left, rationally caused by the additional friction in the sliding bearings of the WEC (which was not possible to specifically measure and therefore not accounted for).

However, the curve fits do have a slope of respectively 1.06 ± 0.04 and 1.04 ± 0.08 for WEC 1 and WEC 2, which is logically larger than the slope of 1 due to increase in friction in the sliding bearings for higher and longer, more surge force bearing, waves. For the error-bars, the uncertainty between the measured and simulated power output was used (see III-B).

The coefficient of determination (R^2) of these fitted curves of WEC 1 and WEC 2 are respectively $R^2_{\text{WEC1}} = 0.95$ and $R^2_{\text{WEC2}} = 0.85$. It is worth noting that the coefficient of WEC 2 is significantly lower, than that of WEC 1, so the measurements show less correlation with the simulations for WEC 2 than for WEC 1.

As expected, the measurements of one wave condition are grouped together in the plot. Noticeable is that the measurements of fair wave conditions mostly lie above the measurements of the moderate wave conditions. This might be caused by larger friction friction forces for fair waves, as the waves were higher there.

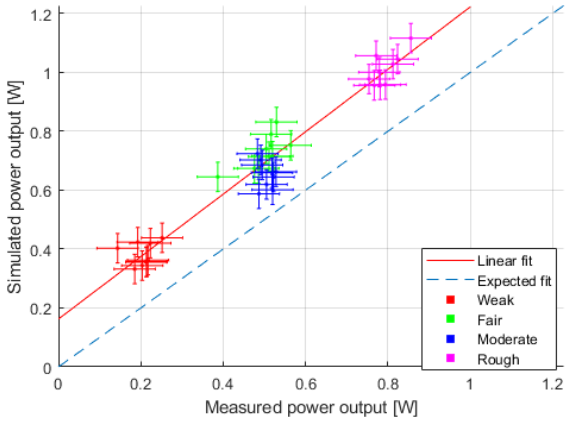

Fig. 14. Comparison of the simulated and measured power output of WEC 1 for every single run.

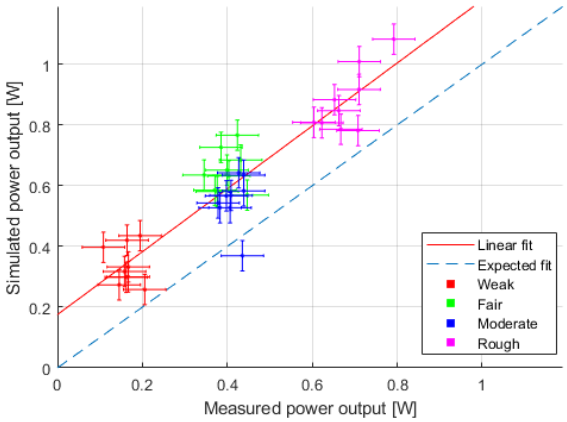

Fig. 15. Comparison of the simulated and measured power output of WEC 2 for every single run.

IV. Discussion

Both numerical and experimental data on interaction of two WECs was generated and evaluated in this paper. This was done for different positions and wave conditions.

F. Error discussion

It can be observed from the experimental results that the damping was not as constant as expected. The dampers had an average damping constant of $\bar{B} = 44.6$ with standard deviation $\sigma_B = 8.7$. The difference between the targeted value of $B_{PTO} = 80$ and the average is acceptable, however the spread in values is problematic. This spread means that the damping, which was to be considered as constant, had to be taken into account as a variable. Even though this variable was easily implemented in the simulations, it made the problem more complex hence more difficult to draw conclusions from the acquired data. Consequently, the q-factor mentioned in III-A could not be computed for the experimental data.

The large variation in the damping constant has likely two possible causes. Firstly, a required damper-mount adjustment after every run could change the friction in the damper system. Secondly, the increasing surge forces on the WEC for larger waves can also increase the friction in the damper.

Within this experiment it was not possible to account for friction forces in the simulation, the friction in the damper is approximated by increasing the damping constant to equalize the net opposing force of one periodic motion.

Unlike the sliding bearing friction, it is possible to account for the damper friction because the load cell measures a combination of the damping and the friction in the damper. This means that an increase of the friction in the damper leads to an increase of the damping constant.

Wave height variations (see table III) originate from imperfections of the wave-maker itself. This variation was accounted for by normalizing P with regard to (h^2). From the simulations the relation between the

power and the wave height for a single WEC was found to be of the form $P(h) = C_{st}h^2$.

This relation was used to normalize the power $\bar{P} = \frac{P}{h^2}$. This method is valid under the assumption that the relation between power and wave height in the experiment is of a similar form. The analysis of all the *sweeps* suggested this as normalization yielded values $\bar{P}$ that were independent of h. Despite the two variables appearing uncorrelated the method might still not be perfectly valid.

G. Interpretation of the results

When analyzing the simulated results for WEC 1, it can be derived that the maximum q-factor of 1.2 for WEC 1 seems to be in accordance with several related studies. For example, a study by Babarit (2010) [14] indicates a maximum q-factor of 1.3 with similar wave conditions. When considering Figure 8 there appears to be a pattern in the power output of WEC 1.

Our hypothesis is that this phenomenon can be linked to the peaks and troughs of the interfering radiation waves of the WECs. A similar pattern of higher and lower energy bands was expected, for different wave conditions. However, the exact dimensions of the pattern is conclusively not validated by the experimental data of WEC 1.

As mentioned earlier, Figure 9 for the simulated power output of WEC 2 as function of the location of WEC 2 is counter-intuitive. The simulation results show a maximum q-factor for WEC 2 of 1.9, which is not in accordance with the related Babarit (2010) study. In addition, the realistic pattern observed for WEC 1 cannot be identified in Figure 9 for WEC 2. Therefore the simulated power output for WEC 2 may be considered as erroneous.

The insight that the simulated results of WEC 1 are more plausible than those of WEC 2, is confirmed by the experimental results as well. When plotting the simulated power output against the experimental power output for WEC 1 we find a fit with a coefficient of determination R^2 of 0.95. Doing the same for the power outputs of WEC 2 the fit has an inferior R^2 of 0.85, as was shown in Figures 14 and 15.

Computational results for WEC 2 show little correlation with our experimental data and literature. This can be due to two possible reasons. First of all, we utilized a BEM solver, NEMOH, to compute the hydrodynamic interaction of both WECs with large relative locations, at some instances. The BEM solver tends to be less accurate at larger domains. However, the errors induced by the BEM solver limitations generally lie within a much smaller range than the errors observed for WEC 2 [15].

Secondly, simulation results for WEC 2 are only realistic at the $\alpha = 90$ configurations, as in that case the power output of WEC 1 equals that of WEC 2 (Figure 10). In all other configurations however, WEC 2 yielded unrealistic simulation results. This leads to the conclusion that the disparities between WEC 2 simulations and literature exhibit that further work with NEMOH and WEC-Sim coupling is needed, for accurately simulating the power production of WEC2, as they have an influence on the estimated power of WEC1.

In addition, since the simulations aim to describe the interaction effects, if the simulated WEC 2 power is incorrect it could have influence on the simulated power of WEC 1 as well.

V. Conclusion

The aim of this study was to provide insight into the influence of the spacial configuration of two generic WECs on their individual power performance. We investigated this both with numerical simulations and experimental testing.

From the simulations, it can be concluded that the individual power output changes when the relative position between to WECs is varied. For WEC 1, the WEC that encounters incident waves first, the change in power output caused by location lead to a maximum q-factor of 1.2. The q-factor is defined as the individual power output of an interacting WEC compared to an isolated WEC.

For WEC 1's computations, a pattern of bands is identified where higher q-factors occurred. These bands are related to higher power output due to the phenomenon of higher local wave heights, induced by the interference pattern caused by the radiation waves between both WECs.

Considering the simulated results of WEC 2, at locations that seem counter-intuitive, unrealistically high q-factors of up to 1.9 were computed, not matching other works of literature. We have reason to believe that those results were caused by a bug in our simulations for WEC 2.

From the experiment, we firstly concluded that the spatial configuration does indeed have an effect on the q-factor. Secondly, the experiment confirmed that the simulation of WEC 1 is more realistic than the simulation of WEC 2.

Finally, due to unexpected variations in the incoming wave height and the PTO damper performance, see section IV-A, it was not feasible to compute appropriate experimental q-factors and thereby validate the spatial dimensions of the patterns observed in the the simulated results (Figures 8 and 9).

Based on the insights acquired during this study, we propose the following recommendations for further research:

- In computing the hydrodynamic interaction between WECs at a larger domain, consider using wave propagation modelling in combination with BEM solvers. This would serve a higher level of accuracy at large domains.
- Attempt to isolate the cause of the incorrect simulation results for WEC 2.
- With respect to our experimental method, we would recommend further research on array configurations to take place in a larger wave flume.

This enables researchers to avoid physical limitations on Deep Sea conditions as well the relative location between WECs in the test basin.

- Use a wave flume with a wave-maker that produces more consistent waves. The effects of the wave height could then be isolated from the experiment.
- Furthermore, regarding the PTO system used in during the experiments, it is recommended for the PTO system to have a fixed damping constant. As is noticed in the analysis, having a varying damping constant during testing, inhibits individual experimental runs to be compared directly.
- In further research, it would be interesting to see validations of the spatial bands of higher and lower power output. Obtaining the knowledge of the exact relative locations of higher energy extraction would be valuable for the actual design of WEC farms.

ACKNOWLEDGEMENT

This research was supported by the department of Maritime and Transport Technology of TU Delft, by making available the wave tank facility for this bachelor thesis. We would like to thank the people involved with this facility for their help during the performance of the experiments.

REFERENCES

[1] K. Gunn and C. Stock-Williams, "Quantifying the potential global market for wave power," in *Proceedings of the 4th ICOE*, Oct. 2012.

[2] EnerData, "Energy statistical yearbook 2017." [Online]. Available: https://yearbook.enerdata.net/electricity/electricity-domestic-consumption-data.html

[3] K. Koca *et al.*, "Recent advances in the development of wave energy converters," in *Proceedings of the 10th EWTEC*, Sep. 2013.

[4] K. O'Brien, "Infrastructure Access Report CETO Unit Hydrodynamic Testing and Validation," FloWave TT / UEDIN Curved Wave Tank, Tech. Rep., 12 2014.

[5] S. D. Chowdhury, R. De La Cruz, T. Huynh, B. Winship, and R. Manasseh, "Computation of power from an array of wave energy converters using a boundary element method," in *Proceedings of the 20th AFMC*, 2016.

[6] P. Balitsky, G. Fernandez, V. Stratigaki, and P. Troch, "Assessing the impact on power production of wec array separation distance in a wave farm using one-way coupling of a bem solver and a wave propagation model," in *Proceedings of the 12th EWTEC*, Aug. 2017, pp. 1176 1–10.

[7] S. Bozzi, M. Giassil, A. M. Miquel, and A. Antonini, "Wave energy farm design in real wave climates: the italian offshore," *Elsevier Energy*, vol. 122, pp. 378–389, 2017.

[8] F. Kalofotias, "Study for the hull shape of a wave energy converter-point absorber," June 2016, master thesis at department of Water Engineering Management University of Twente.

[9] R. Carballo and G. Iglesias, "A methodology to determine the power performance of wave energy converters at a particular coastal location," *Energy Conversion and Management*, vol. 8, no. 18, 2012.

[10] J. Journee and W. Massie, *Offshore Hydromechanics*. Delft University of Technology, January 2001. [Online]. Available: https://ocw.tudelft.nl/wp-content/uploads/OffshoreHydromechanics_Journee_Massie.pdf

[11] A. Techet, "Lecture 4 on 2.016 hydrodynamics," 2005, from Massachusetts Institute of Technology.

[12] A. Babarit and G. Delhommeau, "Theoretical and numerical aspects of the open source bem solver nemoh," September 2015. [Online]. Available: https://lheea.ec-nantes.fr/logiciels-et-brevets/nemoh-presentation-192863.kjsp

[13] N. R. E. Laboratory and S. Corporation, "WEC-Sim User Manual," 2014. [Online]. Available: https://openei.org/w/images/c/c7/WEC_Sim_User_Manual_v1.0.pdf

[14] A. Babarit, "Impact of long separating distances on the energy production of two interacting wave energy converters," *Ocean Engineering*, vol. 37, no. 8, pp. 718 – 729, 2010.

[15] T. Verbrugghe, V. Stratigaki, P. Troch, R. Rabussier, and A. Kortenhaus, "A comparison study of a generic coupling methodology for modeling wake effects of wave energy converter arrays," *Energies*, vol. 10, no. 11, 2017.